AD-A084 187 NAVAL OCEAN SYSTEMS CENTER SAN DIEGO CA F/G 20/4
DIGITAL IMAGE ANALYSIS OF TWO PHASE FLOW DATA.(U)
JAN 80 M M REISCHMAN, J M HOLZMANN
UNCLASSIFIED NOSC-TR-502 NL

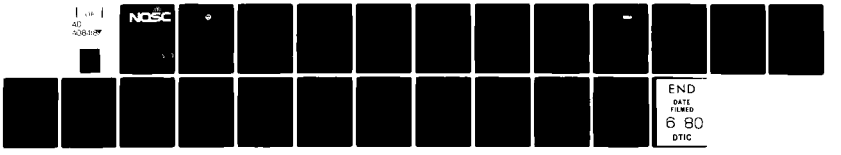

(12) LEVEL II

# NOSC

NOSC TR 502

NOSC TR 502

**Technical Report 502**

# DIGITAL IMAGE ANALYSIS OF TWO PHASE FLOW DATA

MM Reischman and JM Holzmann
(NOSC)
NH Hughes
(San Diego State University Foundation)

15 January 1980

Final Report: FY 79



Approved for public release; distribution unlimited

**NAVAL OCEAN SYSTEMS CENTER**
**SAN DIEGO, CALIFORNIA 92152**

NAVAL OCEAN SYSTEMS CENTER, SAN DIEGO, CA 92152

AN ACTIVITY OF THE NAVAL MATERIAL COMMAND

SL GUILLE, CAPT, USN
Commander

HL BLOOD
Technical Director

## ADMINISTRATIVE INFORMATION

This report describes work which was completed at the Naval Ocean Systems Center (NOSC), San Diego, California. This work was funded by the Independent Research (IR) program of NOSC 638A01 - ZS10.

Released by
J. H. Green, Head
Hydromechanics Division

Under authority of
J. H. Green, Acting Head
Fleet Engineering Department

(14) NOSC-TR-502

UNCLASSIFIED

SECURITY CLASSIFICATION OF THIS PAGE (When Data Entered)

## REPORT DOCUMENTATION PAGE

READ INSTRUCTIONS BEFORE COMPLETING FORM

1. REPORT NUMBER: NOSC Technical Report 502 (TR 502)

2. GOVT ACCESSION NO.: AD-A084787

3. RECIPIENT'S CATALOG NUMBER:

4. TITLE (and Subtitle): Digital Image Analysis of Two Phase Flow Data,

5. TYPE OF REPORT & PERIOD COVERED: Final Report, FY 79, (FOR)

6. PERFORMING ORG. REPORT NUMBER:

7. AUTHOR(s): (10)
M. M. Reischman (NOSC)
J. M. Holzmann (NOSC)
N. H. Hughes (San Diego State University Foundation)

8. CONTRACT OR GRANT NUMBER(s):

9. PERFORMING ORGANIZATION NAME AND ADDRESS:
Naval Ocean Systems Center
San Diego, California 92152

10. PROGRAM ELEMENT, PROJECT, TASK AREA & WORK UNIT NUMBERS:
638A01-ZS10

11. CONTROLLING OFFICE NAME AND ADDRESS:
Naval Ocean Systems Center
San Diego, California 92152

12. REPORT DATE: (11) 15 January 1980

13. NUMBER OF PAGES: ~~20~~ 23

14. MONITORING AGENCY NAME & ADDRESS (if different from Controlling Office):

15. SECURITY CLASS. (of this report): Unclassified

15a. DECLASSIFICATION/DOWNGRADING SCHEDULE:

16. DISTRIBUTION STATEMENT (of this Report)

Approved for public release, distribution unlimited

17. DISTRIBUTION STATEMENT (of the abstract entered in Block 20, if different from Report)

18. SUPPLEMENTARY NOTES

19. KEY WORDS (Continue on reverse side if necessary and identify by block number)
digital image processing
fluid mechanics
hydrodynamics
two phase flow fields

20. ABSTRACT (Continue on reverse side if necessary and identify by block number)

The analysis of flow visualization data documenting a variety of fluid phenomena has been severely limited in the past by the subjective nature of data interpretation and limitations imposed by actual sample size. Video digitization offers a reliable method of automating the analysis of such visual data.

This paper describes an experiment wherein the distribution of sizes of bubbles formed by air injection into a water stream was found. Previous results were limited to special cases due to the amount of data required for a full documentation. Several geometric and flow parameters were varied and their effects are reported.

Data reduction was via a digital image processing system. This type of system holds the promise of high speed, objective data reduction for a broad range of fluid mechanics problems.

DD FORM 1 JAN 73 1473 EDITION OF 1 NOV 65 IS OBSOLETE
S/N 0102-LF-014-6601

UNCLASSIFIED
SECURITY CLASSIFICATION OF THIS PAGE (When Data Entered)

393 157

## INTRODUCTION

Two phase flows are commonplace in hydrodynamic engineering applications. Some examples are heat transfer via gas/water flow in heat exchangers, cavitating hydraulic control systems, and exhaust disposal in underwater vehicles. A particularly bothersome problem in Naval applications is the acoustic nature (i.e., transmissivity and/or reflectivity) of bubble-laden flow fields. The acoustic properties are a function of various factors including bubble density, distribution and size. The purpose of the experimental research performed at the Naval Ocean Systems Center (NOSC) was to quantify the bubble size distributions associated with gas emission into a turbulent boundary layer flow and assess the effects of a variety of flow parameters on the bubble sizes.

Two phase flow fields can be measured in a number of ways: gas content, velocity or pressure fields, bubble properties and bubble dynamics. Suitable electronic methods (laser anemometers, gas content analyzers, etc.) exist for the measurement of most of these variables, but bubble properties (as seen in the flow field) are primarily recorded via movies and/or still photographs. In order to establish the statistical properties of the flow field with reasonable accuracy, a large sample must be obtained, which implies the detailed analysis of many still or movie frames. Data reduction using hand measurement techniques is tedious, but has provided the only data (Reference 1) to date on the expected sizes of bubbles generated when gas is emitted normal to a fluid flow stream. Due to the massive data gathering problem, Silberman's data were restricted to maximum bubble sizes only.

The advent of video digitization and on-line computer analysis permits the efficiency of pictorial data reduction to be greatly increased. In order to overcome past problems, the reduction of the data reported herein was accomplished by the use of video digitization of 16mm movies coupled with subsequent image analysis controlled and performed by an on-line minicomputer. The system expands upon the work of Cornelius, et al. (Reference 2) and represents a first attempt at quantifying vast amounts of visual data. While this report represents a very specific application of the data reduction system, the technique used is very powerful and is applicable to a broad range of fluids engineering problems, such as Corke, et al. and Nagib (References 3 and 4, respectively).

## EXPERIMENTAL

The experiments were performed in the NOSC water tunnel, a high speed (0-19 m/s), low-turbulence ($< 0.1\%$), recirculating facility. The water tunnel is shown schematically in Figure 1. The test section is an open-jet type, with a 30 cm submerged water jet flowing through an octagonal, 1.0 m wide, and 1.2 m long ambient pool of water. A flat plate dividing the flow field was installed in the water tunnel test section. It contained plumbing and passages which allowed air to be ejected from a variety of configurations into the adjacent boundary layer flow. In order to compare the results of separate trials, the velocity field of the flow was carefully characterized with a laser anemometer. During testing the freestream (or approaching flow) velocity (1.5-3.0-m/s) was carefully monitored, as were water temperature (17-18°C), water tunnel pressure (constant at 1.5 $kg/cm^2$) and air bleed rates. The gas flow control system permitted variation of the pressure and flow rate of the gas. Gas flow rates were varied from 50 to 3000 standard $cm^3/min$. The air was continuously vented from the water tunnel in order to keep the oncoming flow bubble-free.

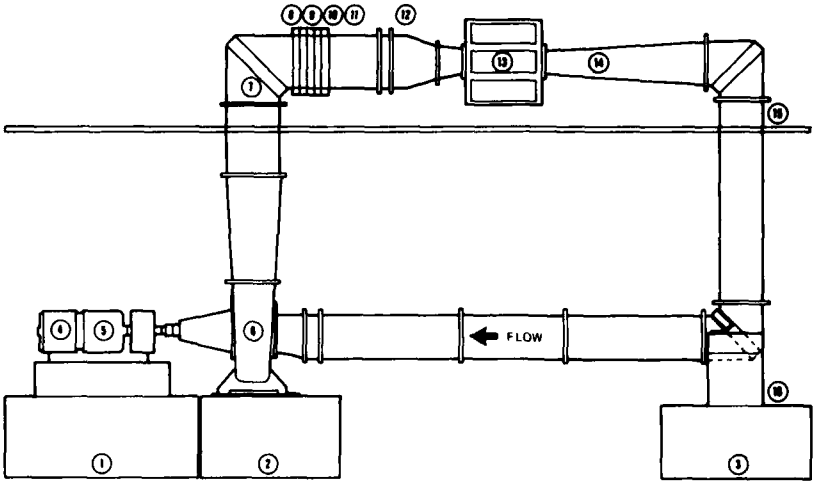


COMPONENTS

1, 2, 3 FOUNDATIONS
4 MOTOR
5 MAGNETIC CLUTCH
6 PUMP
7 TURNING VANES
8 FOAM
9 COARSE HONEYCOMB
10 FINE HONEYCOMB
11 SCREENS
12 CONTRACTION
13 TEST SECTION
14 DIFFUSER
15 SECOND FLOOR LEVEL
16 FIRST FLOOR LEVEL

Figure 1. NOSC recirculating water tunnel.

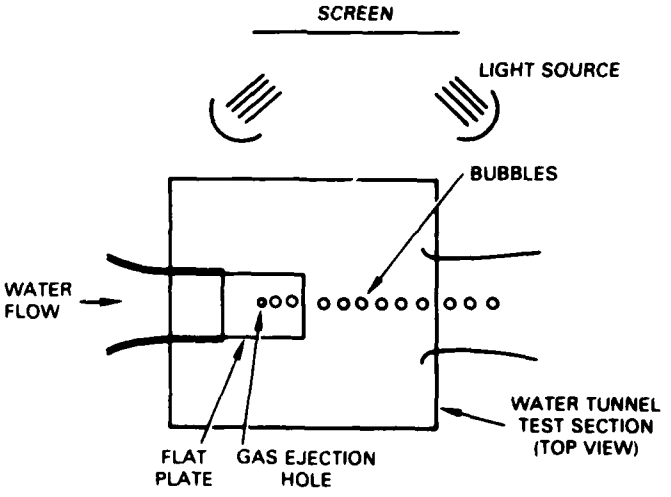


Figure 2. Experimental setup.

The primary means of data gathering, with relation to the bubble characteristics, is photographic. Preliminary lighting experiments showed back lighting to be optimum for contrast. Figure 2 schematically shows the water tunnel test section with flat plate, and the lighting and photographic setup. Both still (35mm) and motion pictures (16mm) were made; the stills were for qualitative viewing and the movies were used in the automatic data reduction scheme. The movies were taken at 50 to 500 frames per second at a distance of approximately 3.5 m. The field of view was intentionally kept small compared to the focal length to minimize parallax errors. The motion picture camera location was duplicated for each run, and the flat plate (of known thickness) was photographed for each test, permitting scaling of the digitized video data.

## DATA REDUCTION

### APPARATUS

The application of video digitization and subsequent on-line computation to fluid flow data is straightforward but unique. A general overview of the instrumentation and data flow is shown in Figure 3. Movies taken in the laboratory are projected by an LW photo optical data analyzer directly into a COHU model 2810 vidicon camera, which is followed by a Datal model ADC-UH8B digitizer. Selected frames are digitized and stored in the frame store memory (Electronic Memories and Magnetic Corp. Micro Ram System 3400N) as a 256 X 256 pixel (picture element) array. Frame store memory is an array of addressable computer memory locations. The moving picture input is monitored on a Tektronix 632 monitor by an operator who makes the decision as to which frames to analyze, avoiding erroneous data points and insuring the independence of data samples. The operator interacts with the system via a *DEC UT 52 Decscope terminal.*

The pictures are enhanced and searched for bubbles. Each bubble is then traced, its area and perimeter found and then converted to real physical dimensions. A three-dimensional shape of the bubble is assumed and its volume estimated. The equivalent spherical diameter of this volume is calculated and stored. Statistics and histograms are extracted from the stored array of equivalent diameters for each set of run conditions. The entire system is controlled by a PDP-11 minicomputer with operator interaction.

### PROGRAM DESCRIPTION

#### Scaling

Relating the size of images produced by the vidicon to actual physical dimensions involves establishing: (1) the relation of apparent X (horizontal) to Y (vertical) dimensions; and (2) the relation of apparent dimensions to actual physical dimensions. To find the X-to-Y ratio scale factor (SCALE), a 7.62 cm X 7.62 cm cross, displayed with its arms parallel to the X and Y axis, is scanned and its X and Y dimensions in pixel units (PU) are determined. Thereafter, all Y dimensions are multiplied by this ratio to convert them to equivalent X dimensions.

Scaling of apparent pixel units to actual dimensions is accomplished by photographing the flat plate thickness on the same film with the bubble pictures. This known dimension (1.79 cm) is scanned with the vidicon and its apparent dimension in pixel units is determined (THI). Multiplying an apparent dimension in pixel units by 1.79/THI converts the dimension to centimeters. Both SCALE and THI are determined several times, and an average is taken.

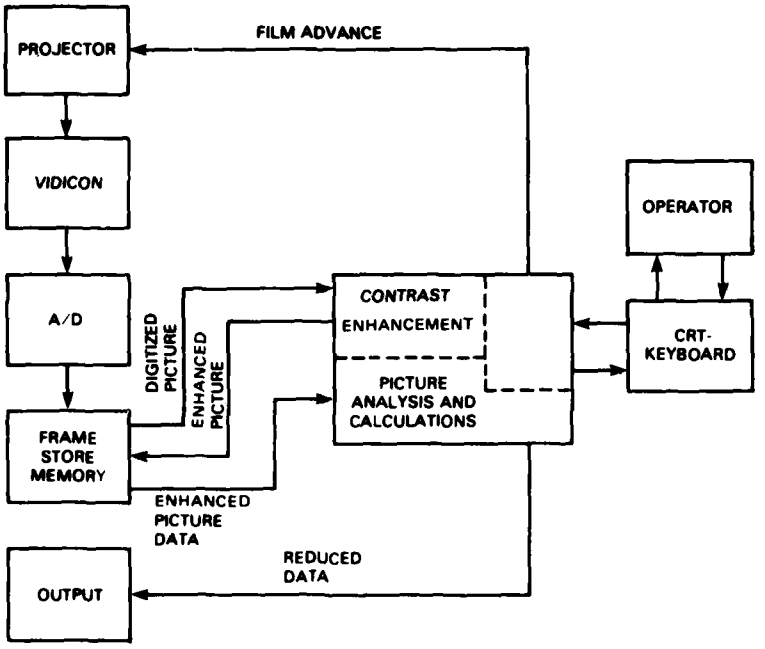


Figure 3. Data flow chart.

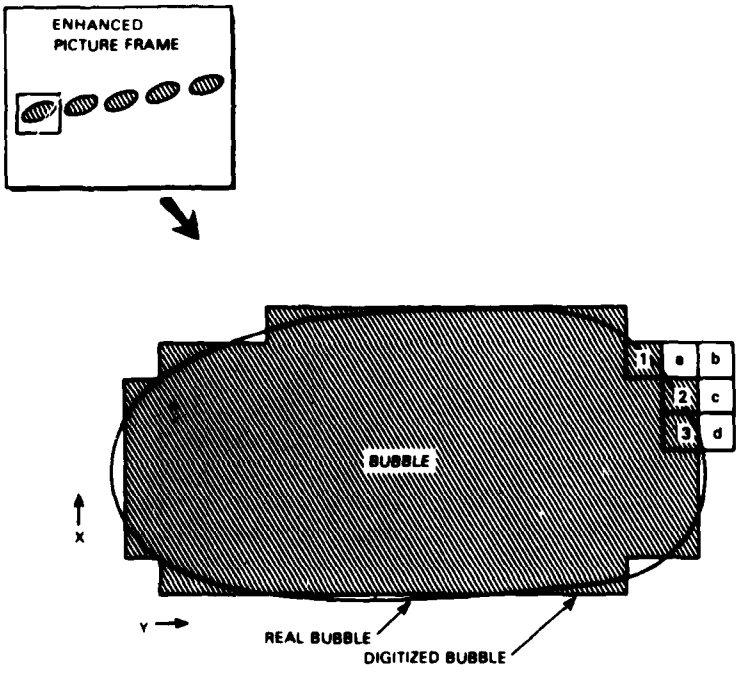


Figure 4. Operation of contour-following routine. Cross-hatched areas are pixels constituting the bubble.

### General Contour Following

Contour following occurs in various forms at several points in the picture analysis program. A general description of the contour-following method is given here and the modifications noted later in the text where appropriate.

The basic contour-following loop is illustrated in Figure 4. From any pixel identified as being on the bubble perimeter, each neighboring pixel is investigated sequentially, clockwise beginning with the previous perimeter pixel. When an adjacent pixel satisfies the perimeter test, it becomes the next perimeter pixel. For example, in Figure 4, the contour-following routine is presently in pixel 2, having moved there from pixel 1. It then tests pixels a, b, c, d, etc., until it finds another perimeter pixel, denoted 3. Having found this perimeter pixel, the routine moves into pixel 3 and begins testing again with pixel c.

### Contrast Enhancement

The contrast of each digitized picture is enhanced to simplify subsequent analysis. Initially each pixel in frame store memory is examined and all non-zero pixels (background) are reassigned the value 128, a medium grey level. The system operator compares this enhanced picture with the original digitized movie frame and can adjust the gain and/or offset of the analog input into the analog/digital converter, store this modified picture in the frame store memory, and begin the enhancement process again. The process is repeated until the operator is satisfied with the fidelity of the bubble shapes shown in the enhanced picture. This same contrast sensitivity level is then used for all frames of that particular data set (Figure 5).

### Picture Analysis

The enhanced pictures in frame store memory are searched for bubbles; each bubble is then analyzed for perimeter length and area and finally an equivalent spherical diameter is calculated. The search routine also includes a method of rejecting old bubbles, i.e., previously examined bubbles.

Each frame is searched from left to right across each line in the array, from top to bottom. A pixel is considered part of the perimeter of a new bubble if its intensity level is lower than that of its neighbor to the left. When a new bubble pixel is encountered, program control passes to the new bubble contour-following routine. This routine traces the contour of the bubble twice. On the first pass, the contour-following routine merely reassigns each pixel immediately adjacent to the bubble the value 175, a light grey level used later in area calculation and bubble discrimination. On the second pass, the program performs pixel column summations to calculate area, computes the perimeters, and reassigns perimeter pixels with 255 (a bright level). (See Figure 5.) As it traces the perimeter pixels, it updates the stored value of area (A) and perimeter (P) by using the exterior pixels previously assigned a level 175.

If the pixel above is equal to 175 (i.e., is an exterior pixel), (A) is increased by the value of the Y coordinate (multiplied by SCALE) of the perimeter pixel; if the pixel below is equal to 175, (A) is decreased by the Y coordinate minus one (times SCALE). The area found in this way is the area enclosed by the exterior edge of the perimeter pixels stored in frame store memory; *but* a more realistic area would be that within a figure formed by connecting the centers of the perimeter pixels (Figure 6a).

To find the area of *this* figure, a correction factor is subtracted from (A) concurrently with each pixel-to-pixel move. This correction factor, always less than one pixel, is determined by the direction of the pixel-to-pixel move and the move previous to it (Figure 6). Concurrently with the area calculation the bubble perimeter is calculated by adding the center-to-center distance of the two pixels in any pixel-to-pixel move. A

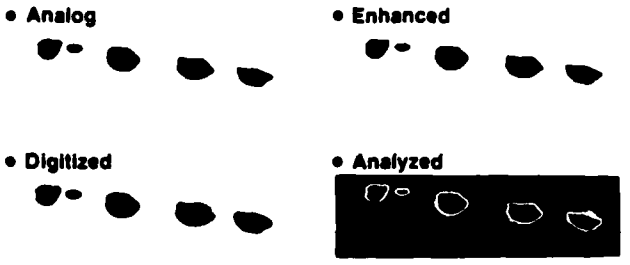


Figure 5. Stages of bubble analysis.

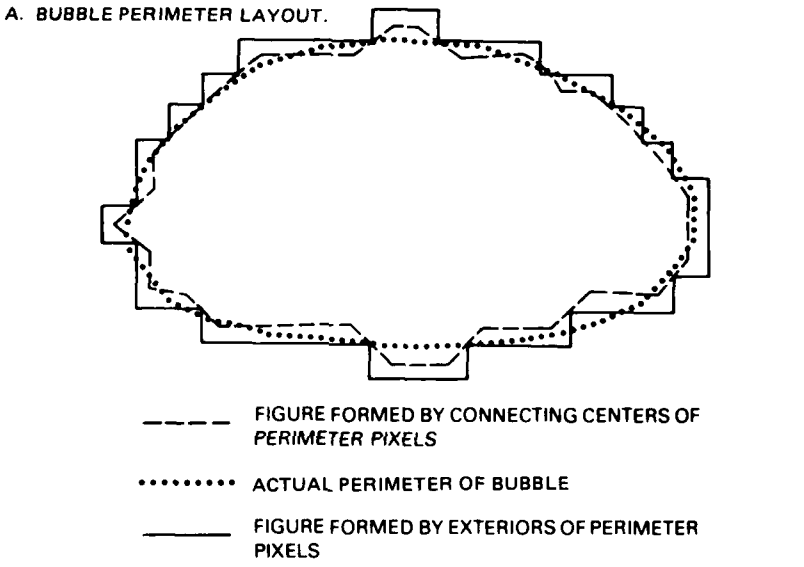


Figure 6. Area correction scheme.

horizontal (X) move increases (P) by one pixel unit, a vertical move by SCALE pixel units (the Y center-to-center distance), and a diagonal move by $(1 + SCALE^2)^{1/2}$. Rigorously, the area and perimeter calculations may be expressed as

$$A = \int_c Y dX \tag{1}$$

and

$$P = \int_c \left(dX^2 + dY^2\right)^{1/2} \tag{2}$$

where both integrations are taken around the contour of a bubble.

Concurrently with the line-by-line search for bubbles, the program looks for pixels of 175 value. Since the only pixels of this value are those immediately adjacent to a previously examined bubble, a 175 identifies an "old bubble." Upon encountering a 175 pixel, the program steps across the bubble until it encounters a 175 pixel followed by a 128 (non-bubble) pixel. This indicates the exterior of the bubble and the program resumes its search across the line.

**Equivalent Diameter Calculation**

The new bubble contour-following program yields bubble perimeter length and area in pixel units and pixel units squared, respectively, which are converted to more common *metric dimensions as follows:*

$$P(cm) = P(pu)\ \frac{1.79\ cm}{THI\ (pu)} \tag{3}$$

and

$$A(cm^2) = A(pu^2)\ \left(\frac{1.79\ cm}{THI\ pu}\right)^2 . \tag{4}$$

Visual studies, substantiated by Reference 5, of plan and elevation view photos of bubbles indicate the shape is predominantly oblate ellipsoidal (i.e., round in plan view and ellipsoidal in elevation). Using the perimeter and area already found, the semi-major, a, and semi-minor, b, axes of the ellipsoid can be found using the following formulae.

$$a = \left\{ \left(\frac{P}{2\pi}\right)^2 + \left[ \left(\frac{P}{2\pi}\right)^4 - \left(\frac{A}{\pi}\right)^2 \right]^{1/2} \right\}^{1/2} \tag{5}$$

and

$$b = \frac{A}{\pi a} . \tag{6}$$

The ellipsoidal volume is

$$V = (4/3)\pi a^2 b, \tag{7}$$

which can be reduced to an equivalent spherical volume of diameter D, where

$$D = 2\left[\frac{3V}{4\pi}\right]^{1/3} . \tag{8}$$

These diameters are stored as an array.

**Statistical Analysis**

The array of bubble equivalent spherical diameters is analyzed with standard statistical methods, that is, the mean and variance are calculated. A probability distribution is found by

$$P(D) = \frac{N(D)}{N_{BUB}} , \tag{9}$$

where

$P(D)$ = probability of a bubble having a diameter between D and D + $\Delta$D
$N(D)$ = number of bubbles having a diameter between D and D + $\Delta$D
$\Delta D$ = largest bubble diameter per data set/100
$N_{BUB}$ = number of bubbles counted.

**Average Bubble Calculation**

The average bubble volume, $V_{AVE}$, in $cm^3$/bubble is determined using the following equation:

$$V_{AVE} = (256\, N_{PIX})\ \frac{1.79}{THI}\ \frac{Q}{U}\ \frac{1}{N_{BUB}} . \tag{10}$$

where

$N_{PIX}$ = number of frames analyzed
$Q$ = gas flow rate ($cm^3$/sec)
$U$ = water tunnel flow velocity, (cm/sec)
256 = digital image width, (pu).

This average bubble volume is used to calculate an average bubble diameter (an experimental value). Because the digital data is suspect in some cases, this average is taken as the mean and is used to correct the standard deviation. (See section immediately following.)

## ERROR ANALYSIS

As noted above, the mean bubble diameter of each data set is found by two distinct methods:

(a) digital image analysis, and

(b) gas flow, number of bubbles counted, etc. (average bubble size).

The error incumbent in calculating the average bubble diameter is dependent on the experimental parameters in Equation 10. Equation 10 is differentiated with respect to each of the parameters, the 95% confidence interval of each parameter is estimated, and the resulting bubble size error is computed. (See Reference 6.) This error varies somewhat from run-to-run and the maximum found was approximately ±6%. For simplicity, this error is taken as the 95% confidence interval on all average bubble size calculations.

For a portion of the data the two methods for bubble size calculation agree quite well (16 data runs below 10% error). However, for the remainder of the reduced data (39 runs), differences between the two computed diameters were as high as 40%.

With large errors present it is useful to know the sources of such discrepancies; whether they are partly photographic or what portion comes from the actual digital image processing. In order to determine an internal digital system error, ellipses of known sizes were drawn and photographed using a 16mm movie camera. These movies were analyzed a number of times via the system and the mean error recorded. This error is presented in Figure 7. The internal system error is small compared to the total error, and one can conclude the photography was the predominant source. (The photographic problems, particularly lighting arrangement and contrast, necessitated processing in such a way that relative bubble sizes are maintained but absolute sizes contain large errors.) It was observed that errors in bubble sizes found via the digital image analysis were consistently biased for any set of data with the same photographic parameters. These photo/video interface problems are very apparent to the system operator, and subsequent comparison of results from the two methods confirms the observation.

The validity of the digital image analysis has been established and in order to provide the most useful and accurate results possible it was decided to use the average bubble sizes, as computed by method b, in the presentation of results. Future refinement of the photographic parameters and photo/video interface would yield digital image results of better quality.

In calculating the standard deviations of the bubble size distributions, a simple correction was applied to the digital image analysis calculation. (The variance could not easily be computed from experimental quantities as the average bubble size was.) It can be shown that if all elements of a set of data are biased by a multiplicative factor, the mean and standard deviation are multiplied by this same factor. By applying this principle to the data obtained by the two methods, the statistical distribution of bubble sizes can be unbiased. The average bubble size (calculated from gas flow rate, etc.) is taken as the real mean, and the standard deviation found from digitized picture analysis is multiplied by $D_a/D_d$.

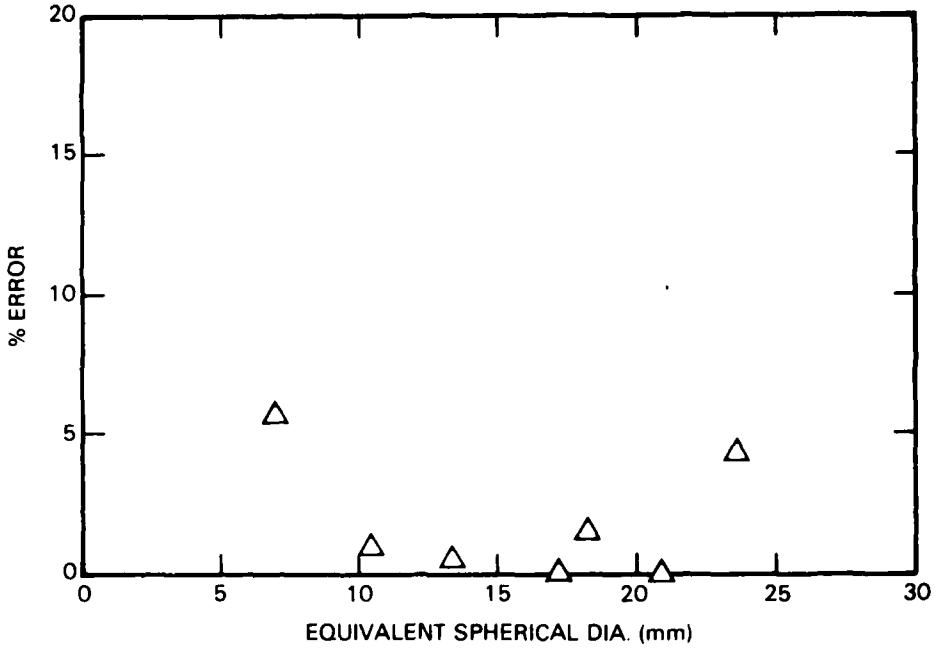


Figure 7. Internal digital system error.

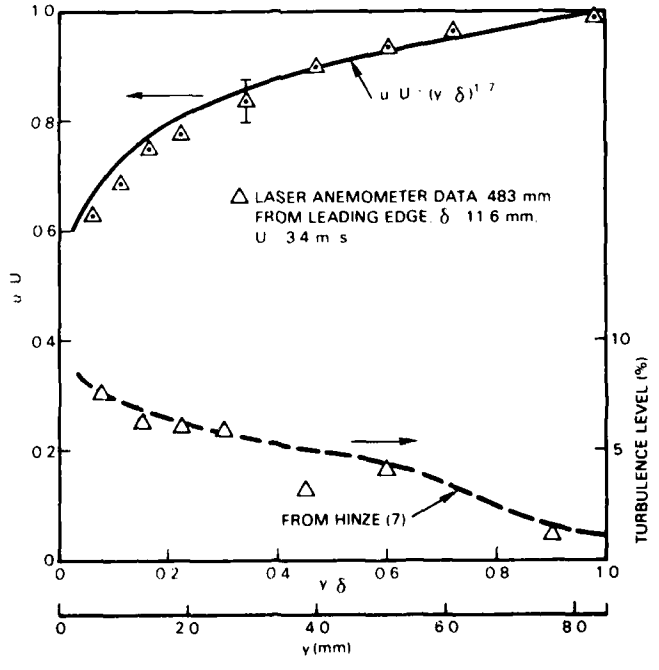


Figure 8. Velocity profile.

where $D_a$ is the average bubble diameter and $D_d$ is the diameter found from the digital processing system.

All data presented (except the histograms in Figure 15) have been corrected by this method.

## RESULTS/DISCUSSION

The initial efforts in the experimental measurements were directed toward characterizing the flow field in which the visual experiments were to be done. The intent was to permit valid comparisons with past and future data of a similar type. As noted earlier, the apparatus was a flat plate whose boundary layer flow properties are well known. Measurements were made of the velocity profile, u (y), and of the turbulent intensities at the air ejection location with a laser Doppler anemometer and were compared with the calculated profile. The results are plotted in Figure 8. The solid line represents the calculated normalized profile using the common 1/7 power law. The boundary layer thickness, $\delta$, was calculated assuming a flat plate flow turbulent from the leading edge and a length Reynolds number of approximately $9 \times 10^5$. The other normalizing variable, U, was measured. The brackets on the data points in this and subsequent figures, unless otherwise noted, will represent the 95% confidence interval. The data and theory are in good agreement.

Figure 9 demonstrates the results of the bubble size measurements in an overall sense, including several ejector geometries and flow parameters. A representative sample of NOSC results are plotted and compared to the past results of Silberman (Reference 1). The bubble diameter is the equivalent spherical diameter, Q is the gas flow per hole, and U is the free stream velocity at the air ejection location. The line represents the empirically validated formulation of Silberman for maximum bubble sizes. The solid portion has been actually validated with experimental data and the dashed portion is merely an extrapolation of his results. (Silberman's data actually extends for approximately two orders of magnitude higher in Q/U than is shown here.) The results compared favorably with those of Silberman, the mean bubble sizes falling uniformly below the projected maximum bubble size line. This comparison further validates the experimental methods and apparent universality of the results. However, at smaller measured bubble sizes the data tends to flatten out.

Results thus far have been general in nature and have corroborated past data. The data reduction system used here permitted much more parametric analysis than was previously possible. Such parametric results are displayed in the next few figures in an attempt to isolate various critical variables. Figure 10 graphically shows the effect of gas flow on the generated bubble sizes. One should also note that the air ejection hole diameter varies. There is no evidence that the bubble sizes depend uniquely on gas flow rate, Q, or hole diameter. Silberman's line is shown again for reference.

Similarly, in Figure 11 the dependence of bubble diameter on free stream velocity, U, is seen. Again, three hole diameters were used. The water tunnel velocity could only be varied over a factor of about two before an instability developed in the flat plate apparatus, hence two values of constant water flow have been used. No distinct effects of free stream velocity can be seen but further examination over a broader velocity range should be done before conclusive comparisons are made. Both Figures 10 and 11 have

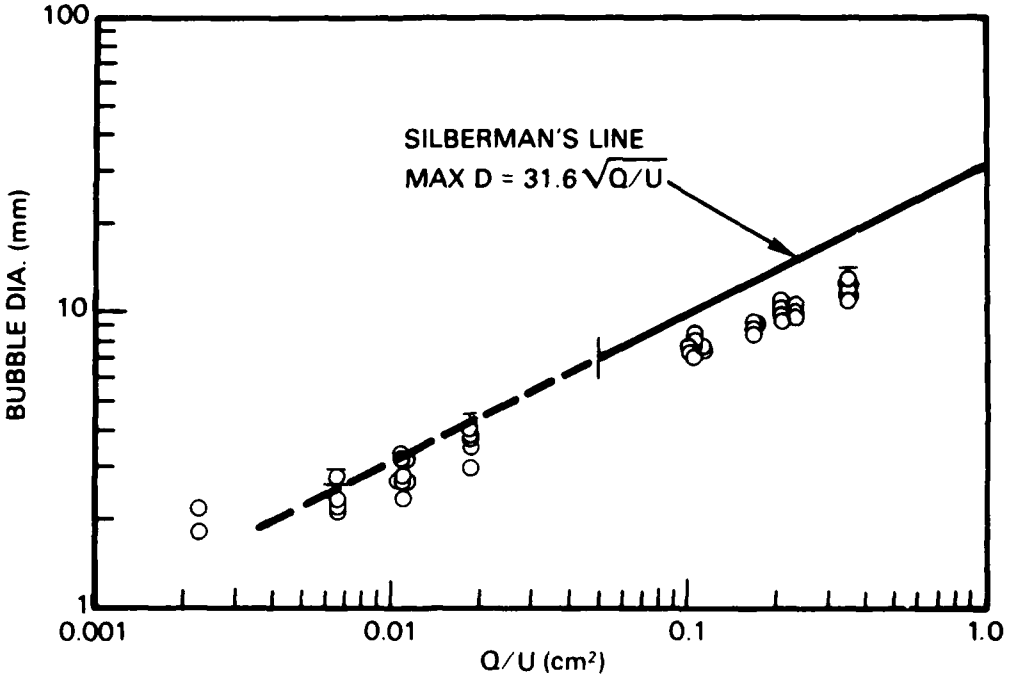


Figure 9. Mean bubble diameter as a function of Q/U: all data.

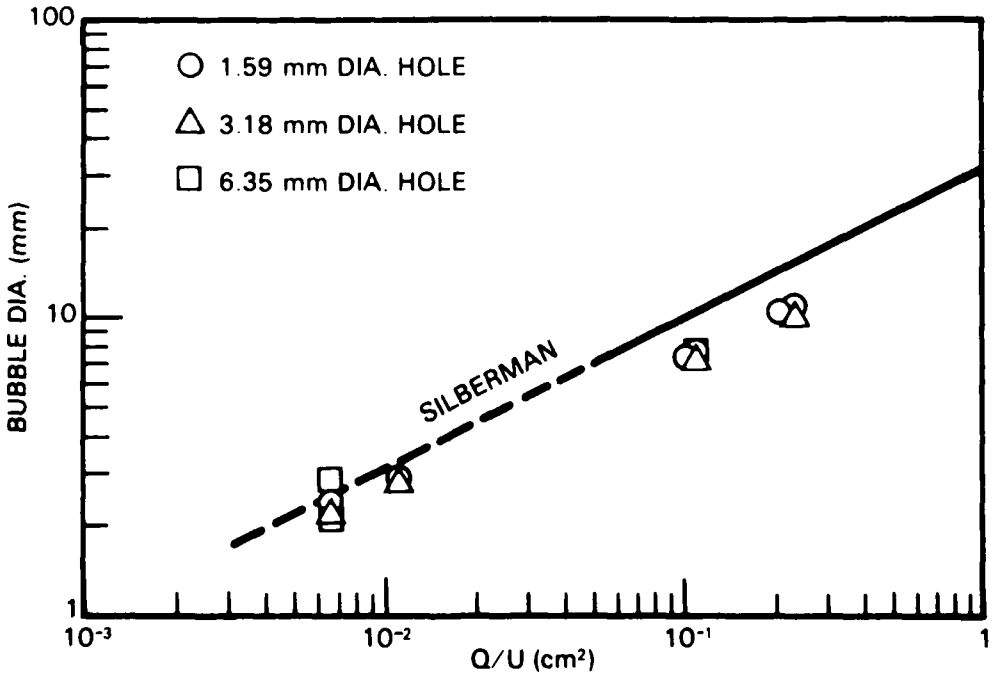


Figure 10. Mean bubble diameter as a function of Q/U: U = constant.

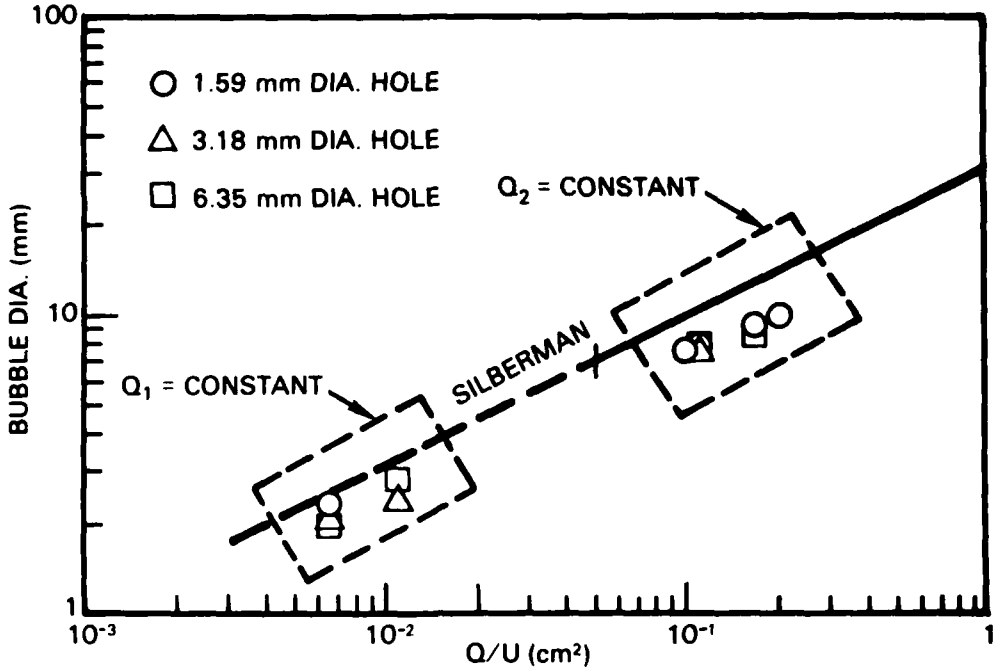


Figure 11. Mean bubble diameter as a function of Q/U: $Q_1$ and $Q_2$ = constant.

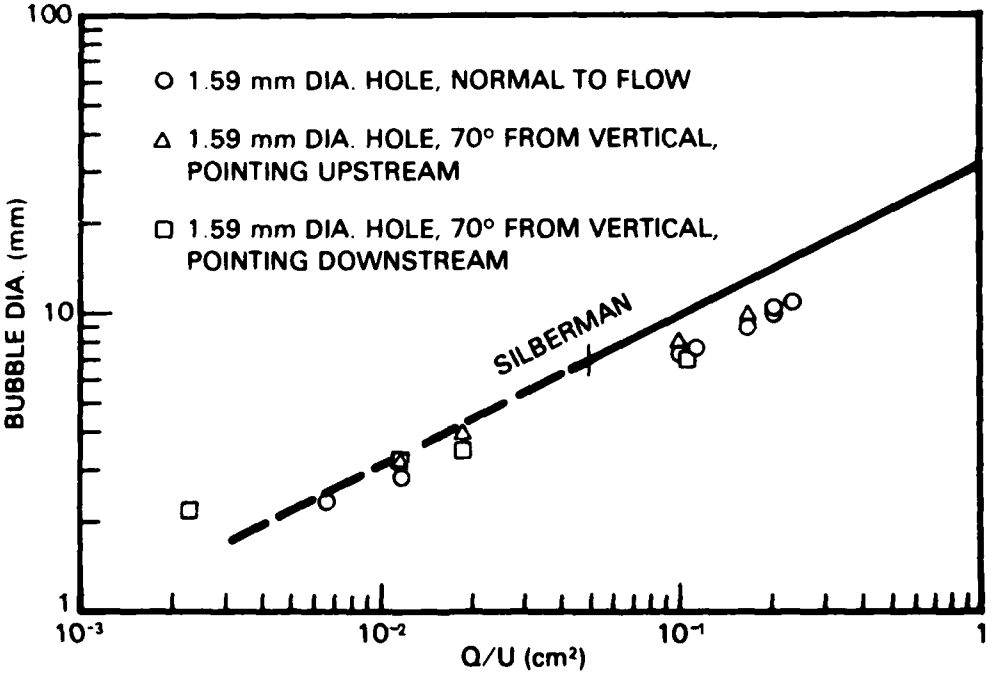


Figure 12. The effect of hole orientation on mean bubble diameter.

shown solid verification of Silberman's finding that hole diameter does not affect the generated bubble sizes, at least not in the regimes investigated. (Silberman's hole diameters were 0.08 to 1.27 cm.)

A number of geometric factors were also considered in the experiments discussed here, namely, number and orientation of holes. Additionally, the effects of a modified boundary layer flow, i.e., changed shear stress and turbulence level, were noted. The results are shown in Figures 12 through 14. The effect of air ejection hole orientation with respect to the approach water flow can be seen in Figure 12. All hole orientation trials were done using a 1.59 mm hole either vertical or 70° from vertical. No clear cut effects on bubble diameter can be noted.

The effects of multiple holes and their arrangement were also studied, albeit in a limited sense. From 2 to 5 holes (either 3.18 or 1.59 mm diameter and oriented normal to the flow) were tried with the line through their centers oriented parallel to and perpendicular to the approach flow. For the perpendicular orientation, visual observations showed that the gas stream from each hole did not interact with the others. Figure 13 displays bubble sizes generated when holes are oriented parallel to the flow stream. One should note the lack of multiple hole data at the lower Q/U values. This was due to an observed intermittent hole flow apparently caused by the cycling of surface tension and internal pressure forces in the air ejection process. Further experiments at higher velocities would be useful. At higher gas flow rates, the same problem existed but to a lesser extent, hence only data from the two-hole cases are presented in Figure 13. The data do not indicate a significant trend. Most importantly, within the range of flow variables investigated here, no bubble agglomeration or mixing was observed in the experiments or in subsequent films. One would anticipate that, in the limit, as free stream velocity increases and boundary layer thickness decreases, the bubbles ejected from separate holes would interact.

External flow field property effects were also examined by modifying the adjacent boundary layer flow. The modification was accomplished by placing a 1.52 mm tripwire near the leading edge of the flat plate apparatus. This abrupt, chaotic boundary layer trip created a thicker (by approximately 50%), and more energetic (more turbulent) boundary layer. The results of measurements made in these circumstances are shown in Figure 14. The data appear to collapse as in past plots and no discernible trends can be seen. However, as free stream velocity is increased beyond current levels (lower Q/U's), it is reasonable to expect that a lower limit on the bubble sizes generated would be approached.

Measurements made to date have only been concerned with the bubble sizes generated and not with the distribution of those sizes. The data reduction technique used here allows such measurements. Typical results are presented in Figure 15. The computed probability distribution is plotted and compared with a Gaussian distribution having the same mean and standard deviation. The calculated mean is also compared with the "diameter of the average bubble," an experimental quantity discussed earlier. Results shown in Figure 15b are atypical but represent the inappropriateness of the Gaussian representation in some cases. The distribution in this case was clearly bimodal and represented a combination of low velocity and very low gas flow. The reasons for the bimodal nature are unclear at this time.

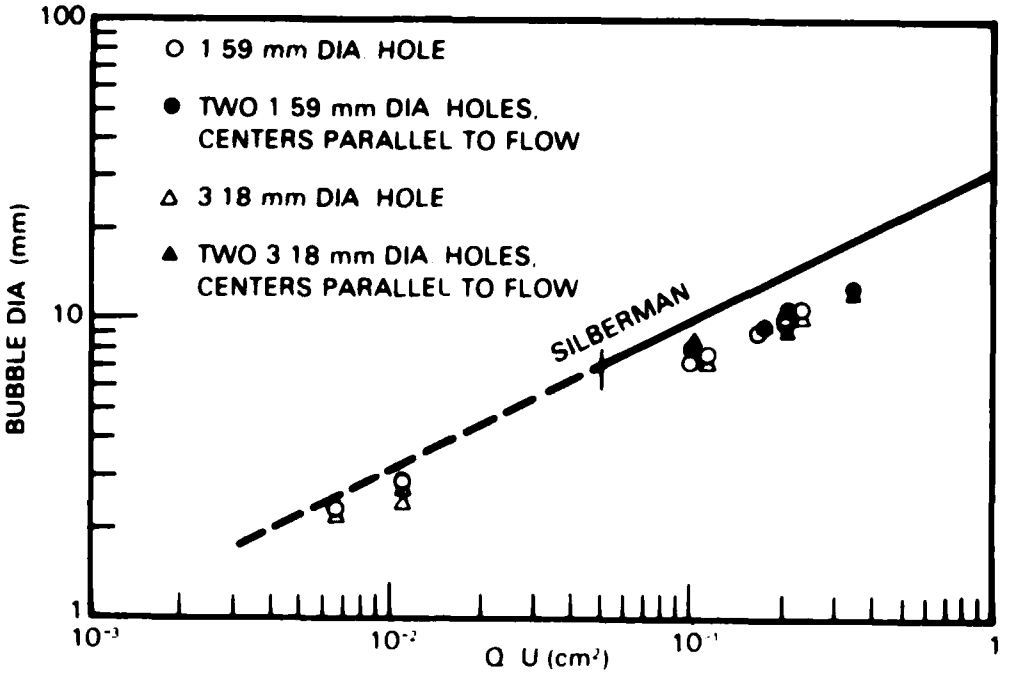


Figure 13. The effects of two hole vs one hole on mean bubble diameter.

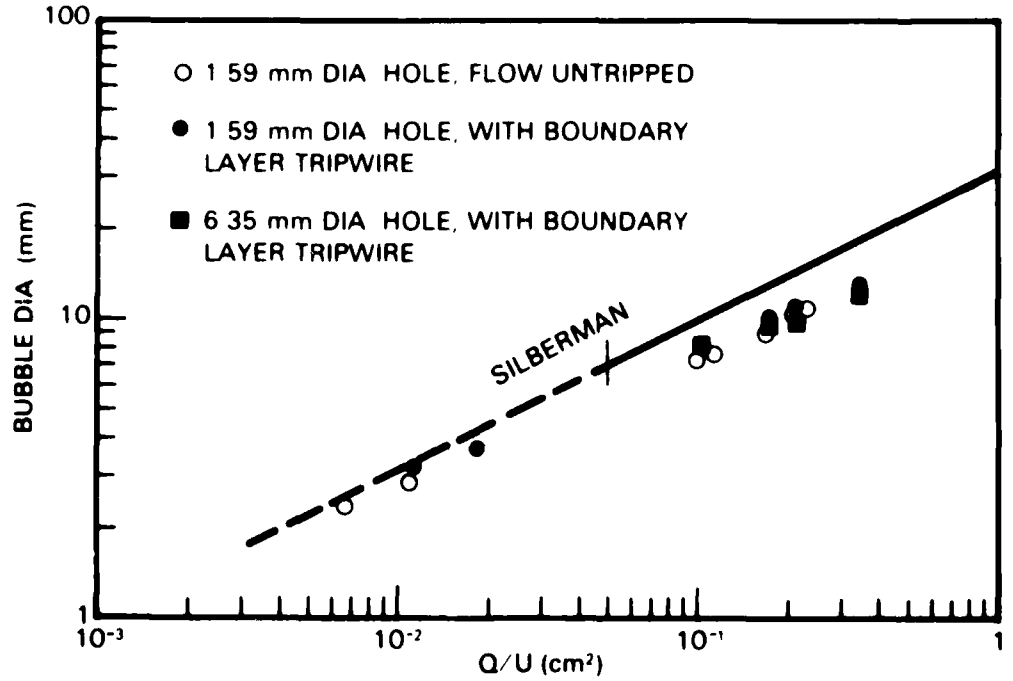


Figure 14. The effect of boundary layer tripwire on mean bubble diameter.

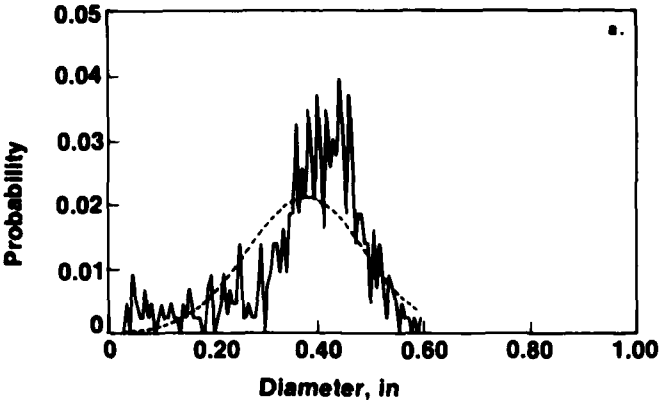


**Mean = 0.3723 Standard deviation = 0.111905**

**Q = 0.890E-03 ft³/sec U = 4.91 ft/sec Q/U = 0.181E-03 ft²**
**Diameter of the average bubble 0.3542**

**1/16 in diameter hole**

**Test number 4 Run number 7**

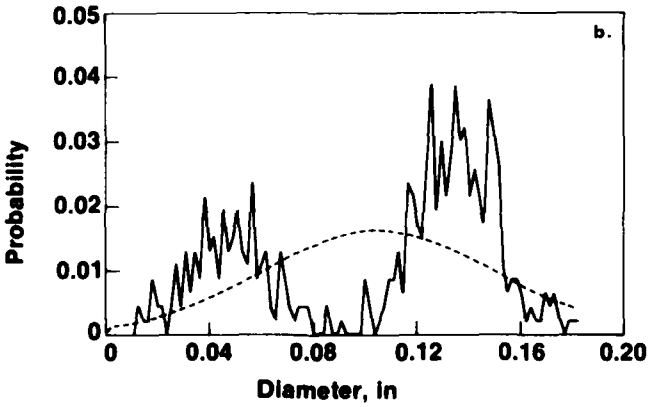


**Mean = 0.1047 Standard deviation = 0.044894**

**Q = 0.578E-04 ft³/sec U = 4.91 ft/sec Q/U = 0.118E-04 ft²**
**Diameter of the average bubble 0.0939**

**1/8 in diameter hole**

**Test number 3 Run number 2**

Figure 15. Typical bubble size distributions.

In order to tie the magnitude of the standard deviation of the bubble diameters to the empirical variable Q/U, the standard deviations associated with data shown in Figures 10 and 11 are plotted in Figures 16 and 17. Hole diameter still appears to be an unimportant variable. It should be noted that the error in $\sigma$ will increase as bubble diameter decreases, largely due to the increasing error in bubble size determination. But the trend is clear, the absolute value of $\sigma$ decreases as Q/U decreases, regardless of the bubble distribution. In practice, the detailed knowledge of the distribution would be of great value but no such generalization can be drawn herein.

Attempts were made to better correlate the standard deviation with other parameters, such as turbulent boundary layer frequency content, and provide a more useful guideline for the engineer or designer using an air ejection system. The most fruitful attempt is shown in Figure 18 where the standard deviation is normalized with the mean value and plotted as a function of Q/A , where A is the ejection hole area. (Q/A also represents the air jet velocity.) All the standard deviations associated with the data in Figures 10 and 11 are included in Figure 18. The data collapse is good and an interesting minimum is noted in the data. This minimum creates for the designer an extra capability and could be very important in the design of specific gas ejection systems.

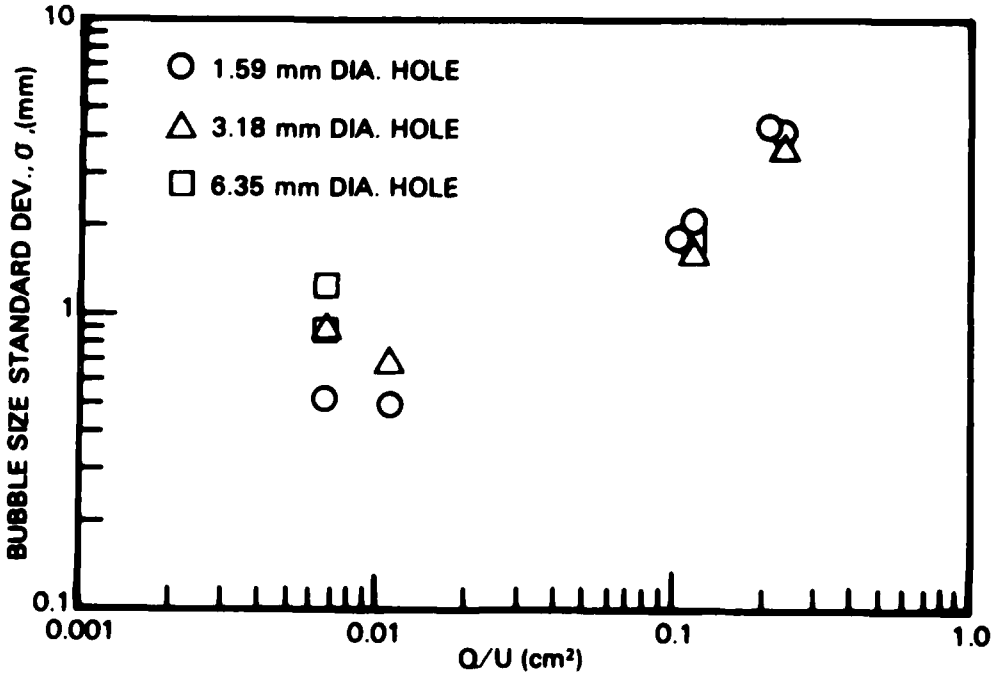


Figure 16. Bubble size standard deviation as a function of Q/U: U = constant.

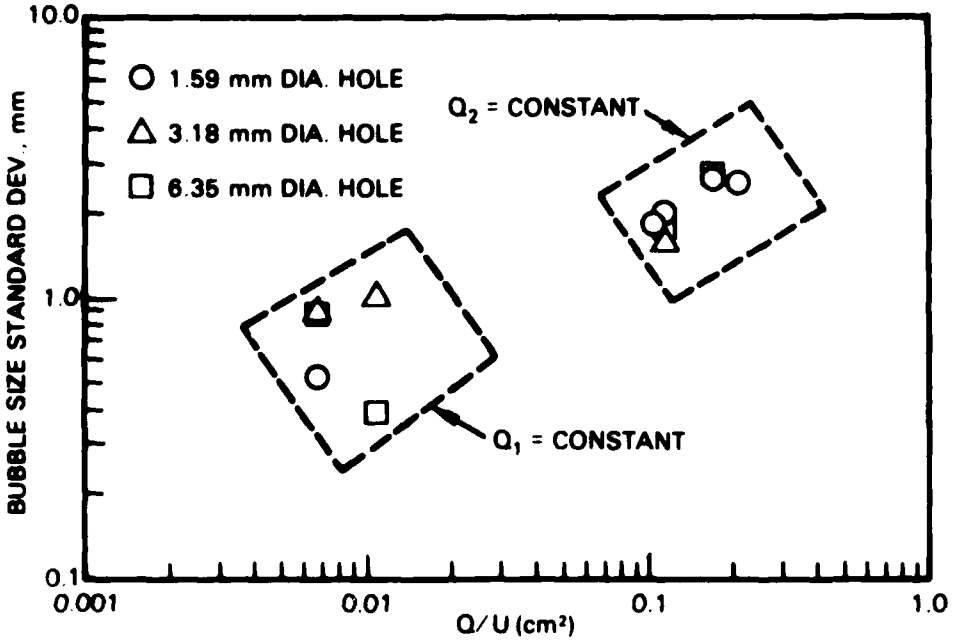


Figure 17. Bubble size standard deviation as a function of Q/U: $Q_1$ and $Q_2$ = constant.

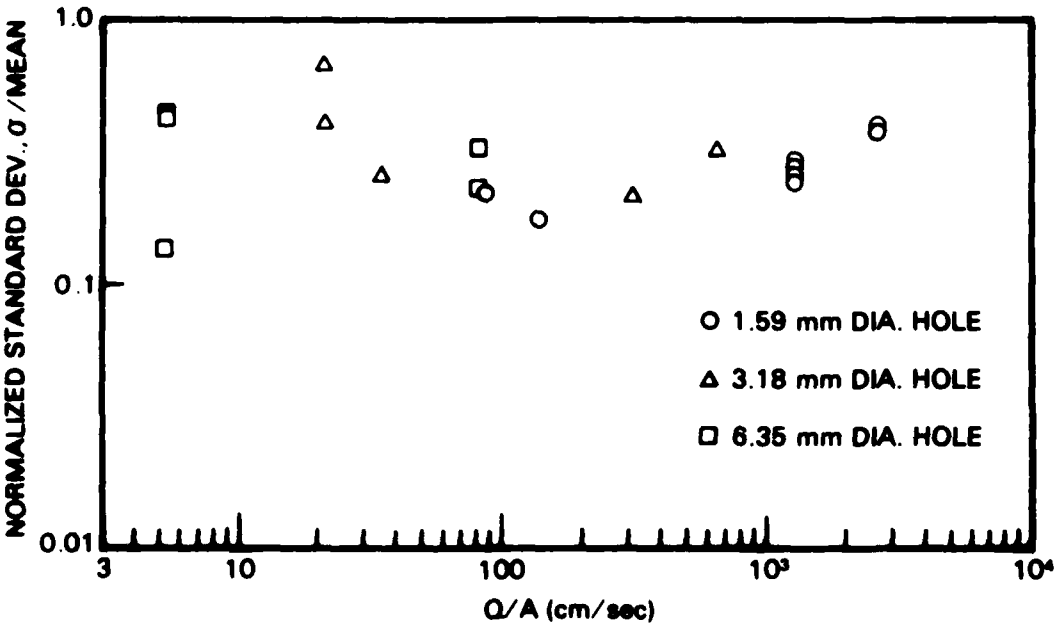


Figure 18. Normalized standard deviation as a function of Q/A: both U and Q constant.

## CONCLUSIONS

An experimental study was conducted wherein the sizes of bubbles generated by gas being ejected into a turbulent boundary layer flow were measured. The experiments were conducted in a low turbulence, recirculating water tunnel using a standard flat plate flow geometry. Results were compared to the previous work of Silberman (Reference 1), but much more data analysis could be accomplished because of the use of video digitization and digital image processing in the present work. The scope of the experimental data summarized below was possible with the use of such advanced data processing techniques. Appropriately enough, a major conclusion of this work should be that *the use of digital image analysis in quantifying the physical processes described by predominantly visual results of flow fields should be extensively exploited.* In most cases where visual results of a high contrast nature can be obtained, the digital image processing of those results would yield more accurate and more extensive data sets.

Other conclusions regarding the nature of the flow field itself can also be drawn from the results discussed in the previous section. These conclusions are as follows:

1. The parameter $(Q/U)^{1/2}$ has been confirmed as an indicator of mean bubble diameter. Silberman had previously found such a dependence for maximum bubble sizes over a higher range of Q/U. At small values of Q/U ($\sim 10^{-2}$ cm$^2$), the mean bubble diameter variation tends to flatten out, but the exact trend has not been established.

2. The isolation of Q and U effects in the bubble generation did not indicate a dominance of either. Gas flows were tested over an adequate range but velocity was varied only over a factor of 2.

3. There appears to be no hole-diameter dependence on the mean bubble size generated, again confirming Silberman's findings for maximum sizes and higher values of Q/U. The effect of hole diameter on the exact nature of the distribution (i.e., bimodal, uniform, Gaussian, etc.) is not clear at this time.

4. The angle of the air ejection hole with respect to the oncoming flow has no influence on mean bubble diameter.

5. The effect of multiple holes and their orientation has been partially uncovered. There appeared to be no interaction between gas flows from holes whose centers were aligned perpendicular to the flow stream. Similarly, but over a limited range of Q/U, holes aligned parallel to the flow direction had no interaction of their individual gas streams. However, a threshold phenomenon of intermittent flow was noted when multiple holes were used. That is, pressure and surface tension forces acting on the gas ejection from multiple holes must be taken into account before bubble size estimations for such a gas ejection system are made.

6. The influence of an upstream boundary layer trip and accompanying increased boundary layer thickness, turbulence level, and wall shear stress on mean bubble sizes generated was negligible.

7. The standard deviation of bubble sizes decreased as the value of Q/U decreased, but the distribution shape does not remain constant. Some evidence is seen of bimodal distributions of bubble sizes at low values of Q/U. When $\sigma$ is divided by the mean diameter and plotted as a function of Q/A, data collapse is good and a local minimum is noted at Q/A $\sim$ 200 cm/sec.

## REFERENCES


1. Silberman, E., "Production of Bubbles by the Disintegration of Gas Jets in Liquids," Presented at the 5th Midwestern Conference on Fluid Mechanics, University of Michigan, 1957.

2. Cornelius, K., Takeuchi, K., and Deutsch, S., "Turbulent Flow Visualization. A Technique for Extracting Accurate Quantitative Information," Presented at the 5th Biennial Symposium on Turbulence, University of Missouri–Rolla, October 3-5, 1977.

3. Corke, T., Koga, D., Drubka, R., and Nagib, H., "A New Technique for Introducing Controlled Sheets of Smoke Streaklines in Wind Tunnels." Proceedings of International Congress on Instrumentation in Aerospace Simulation Facilities, IEEE Publication 77 CH1251-8 AES, 1977.

4. Nagib, H. M., "Visualization of Turbulent and Complex Flows Using Controlled Sheets of Smoke Streaklines." Proceedings of the International Symposium on Flow Visualization, Tokyo, Japan, 1977.

5. Haberman, W., Morton R., "An Experimental Investigation of the Drag and Shape of Air Bubbles Rising in Various Liquids," David W. Taylor Model Basin, Report 802, September, 1953.

6. Barry, B. A., *Engineering Measurements*, John Wiley & Sons, 1964.

7. Hinze, J. O., *Turbulence*, McGraw-Hill, New York, 1959.